nanomaterials

MDPI

Article

Chemical Vapor Deposition of Uniform and Large-Domain Molybdenum Disulfide Crystals on Glass/Al_2O_3 Substrates

Qingguo Gao [1,*], Jie Lu [2], Simin Chen [1], Lvcheng Chen [1], Zhequan Xu [1], Dexi Lin [1], Songyi Xu [1], Ping Liu [1], Xueao Zhang [2], Weiwei Cai [2] and Chongfu Zhang [1,3]

[1] School of Electronic Information, University of Electronic Science and Technology of China Zhongshan Institute, Zhongshan 528402, China
[2] College of Physical Science and Technology, Xiamen University, Xiamen 361005, China
[3] School of Information and Communication Engineering, University of Electronic Science and Technology of China, Chengdu 611731, China
* Correspondence: gqgemw@163.com

Abstract: Two-dimensional molybdenum disulfide (MoS_2) has attracted significant attention for next-generation electronics, flexible devices, and optical applications. Chemical vapor deposition is the most promising route for the production of large-scale, high-quality MoS_2 films. Recently, the chemical vapor deposition of MoS_2 films on soda-lime glass has attracted great attention due to its low cost, fast growth, and large domain size. Typically, a piece of Mo foil or graphite needs to be used as a buffer layer between the glass substrates and the CVD system to prevent the glass substrates from being fragmented. In this study, a novel method was developed for synthesizing MoS_2 on glass substrates. Inert Al_2O_3 was used as the buffer layer and high-quality, uniform, triangular monolayer MoS_2 crystals with domain sizes larger than 400 μm were obtained. To demonstrate the advantages of glass/Al_2O_3 substrates, a direct comparison of CVD MoS_2 on glass/Mo and glass/Al_2O_3 substrates was performed. When Mo foil was used as the buffer layer, serried small bilayer islands and bright core centers could be observed on the MoS_2 domains at the center and edges of glass substrates. As a control, uniform MoS_2 crystals were obtained when Al_2O_3 was used as the buffer layer, both at the center and the edge of glass substrates. Raman and PL spectra were further characterized to show the merit of glass/Al_2O_3 substrates. In addition, the thickness of MoS_2 domains was confirmed by an atomic force microscope and the uniformity of MoS_2 domains was verified by Raman mapping. This work provides a novel method for CVD MoS_2 growth on soda-lime glass and is helpful in realizing commercial applications of MoS_2.

Keywords: MoS_2; chemical vapor deposition; substrate; glass

Citation: Gao, Q.; Lu, J.; Chen, S.; Chen, L.; Xu, Z.; Lin, D.; Xu, S.; Liu, P.; Zhang, X.; Cai, W.; et al. Chemical Vapor Deposition of Uniform and Large-Domain Molybdenum Disulfide Crystals on Glass/Al_2O_3 Substrates. *Nanomaterials* **2022**, *12*, 2719. https://doi.org/10.3390/nano12152719

Academic Editor: Ki Kang Kim

Received: 22 July 2022
Accepted: 3 August 2022
Published: 7 August 2022

1. Introduction

Two-dimensional transition metal dichalcogenides materials, specifically molybdenum disulfide (MoS_2), have emerged as an extremely important candidate for low-power, high-performance, and flexible electronics [1–7]. In order to achieve industry applications, batch production of high-quality and large-scale MoS_2 films at low cost has become a major requirement. Chemical vapor deposition (CVD) has demonstrated great potential in the large-scale production of high-quality MoS_2 films [8–11]. At present, CVD growth of large-area MoS_2 continuous films larger than 4 inches and the deposition of single MoS_2 domains with sizes up to the millimeter-scale have been realized by independent research groups [8–10,12–15], which greatly promote the industrialization process of MoS_2. Although those encouraging advancements have been made in the CVD growth of MoS_2, related studies are still at an early stage for the industrialization of MoS_2 films [16–18]. For example, the size of CVD-grown, single-crystalline graphene has reached up to the meter-scale with very fast growth rates [19,20]. However, there is an obvious gap between CVD MoS_2 and graphene both in crystal size and quality [14,15]. More efforts should be

made on designing a new growth set-up, searching for possible catalysts and promoters, testing appropriate growth substrates and carefully optimizing the CVD growth parameters to lower the cost and improve the quality and uniformity of CVD MoS_2 [18,21].

Recently, low-cost soda-lime glass has been utilized as a growth substrate for CVD MoS_2 growth [12,22–28]. In 2017, Chen et al. synthesized large-size MoS_2 crystals on molten glass at 1050 °C [27]. In 2018, Gao et al. synthesized high-quality bilayer MoS_2 with domain sizes up to 200 μm on molten glass at 830 °C [25]. Zhang et al. reported single-crystal monolayer MoS_2 grown on molten glass at 850 °C with a domain size larger than 500 μm [24]. Yang et al. from Peking University developed a face-to-face metal precursor supply approach and deposited 6-inch uniform monolayer MoS_2 on the glass [12]. In 2020, Zeng et al. demonstrated bandgap tuning of MoS_2 grown on molten glass by a sphere diameter engineering technique [23]. In 2022, Li et al. reported the evolution of crystalline morphology of MoS_2 grown on glass substrates and provided an effective approach to engineering the morphology of MoS_2 crystals [22]. Commonly, due to the growth temperature of MoS_2 being higher than soda-lime glass's melting point, a piece of Mo foil or graphite needed to be used as a buffer layer between the glass substrates and the CVD system in those works to prevent the adhesion of glass substrates and CVD systems [25–27]. However, the MoS_2 morphology and domain size may be critically affected by Mo foil because Mo foil also could be used as the Mo-source in the chemical vapor deposition process [26]. In addition, Mo foils and graphite are very easy to react with oxygen at high growth temperatures, which limits the research approaches to MoS_2 growth on glass substrates, although oxygen has been proven to be an effective gas for improving the size and quality of MoS_2 crystals [8,9,29–32]. For example, Zhang's group obtained a 4-inch monolayer MoS_2 film on a sapphire substrate by epitaxial growth using an oxygen-assisted method [13]. Hence, for the aim of Mo-source precise control and to extend the capability of glass substrates for high-quality MoS_2 CVD growth at variable critical experimental conditions, a non-active buffer layer needs to be explored.

In this work, high-quality CVD monolayer MoS_2 films grown on glass/Al_2O_3 substrates were explored. Firstly, to demonstrate the advantages of glass/Al_2O_3 substrates, MoS_2 films were synthesized on glass/Al_2O_3 and glass/Mo substrates and characterized with optical microscopy in different regions. At the center of the glass/Mo substrates, serried bilayer seeds could be observed on the monolayer MoS_2 domains, while the MoS_2 domains grown on glass/Al_2O_3 substrates exhibited a uniform contrast. At the edge of the glass/Al_2O_3 substrates, monolayer MoS_2 domains with low nucleation density and uniform contrast were grown. As a control, monolayer MoS_2 domains with high nucleation density and multi-layer nucleation sites were grown on the edge region of glass/Mo substrates. Subsequently, the grown MoS_2 thin films were successfully transferred onto SiO_2/Si substrates and characterized with Raman and photoluminescence (PL) spectroscopy, as well as atomic force microscopy (AFM). A comparison of Raman and PL spectra of MoS_2 domains grown by those two methods further illustrates the advantages of the non-active buffer layer, where uniform MoS_2 domains were synthesized as a result of a onefold supply of Mo-source. Finally, the thickness and uniformity of MoS_2 domains on glass/Al_2O_3 substrates were confirmed by AFM and Raman mapping.

2. Experiments and Methods

As depicted in Figure 1, the MoS_2 crystals were grown in a CVD system with a 2-inch-diameter quartz tube and two individual furnaces. In this system, the temperatures of substrates and precursors, carrier gas flow rate, total pressure, and the weight of precursors could be controlled independently. Following the general conditions reported in previous literature [24,25], 1.4 g of sulfur powder and 2 mg of MoO_3 powder were weighed out and placed into separate boats. The boats were placed 25 cm apart in separate regions of the quartz tube to achieve the different temperatures for the S and Mo precursors. Both glass substrates and the buffer layers (Mo foils or Al_2O_3 lamina) were cleaned with acetone (10 min), isopropanol (10 min) and deionized water (10 min). The size of both the substrates

and buffer layers was 20 mm × 20 mm. After loading precursors and substrates, the tube was first pumped down to 0.2 mBar and then filled with Ar to 1000 mBar. The pumping and filling processes were repeated three times to eliminate air and other containment gases in the quartz tube. After that, the temperatures of furnaces I and II were set to 200 and 1050 °C, respectively, with a ramping rate of 10 °C/min. During the growth, high-purity argon was loaded with a flow rate of 20 sccm. After a growth period of 10 min, the furnaces were naturally cooled to room temperature.

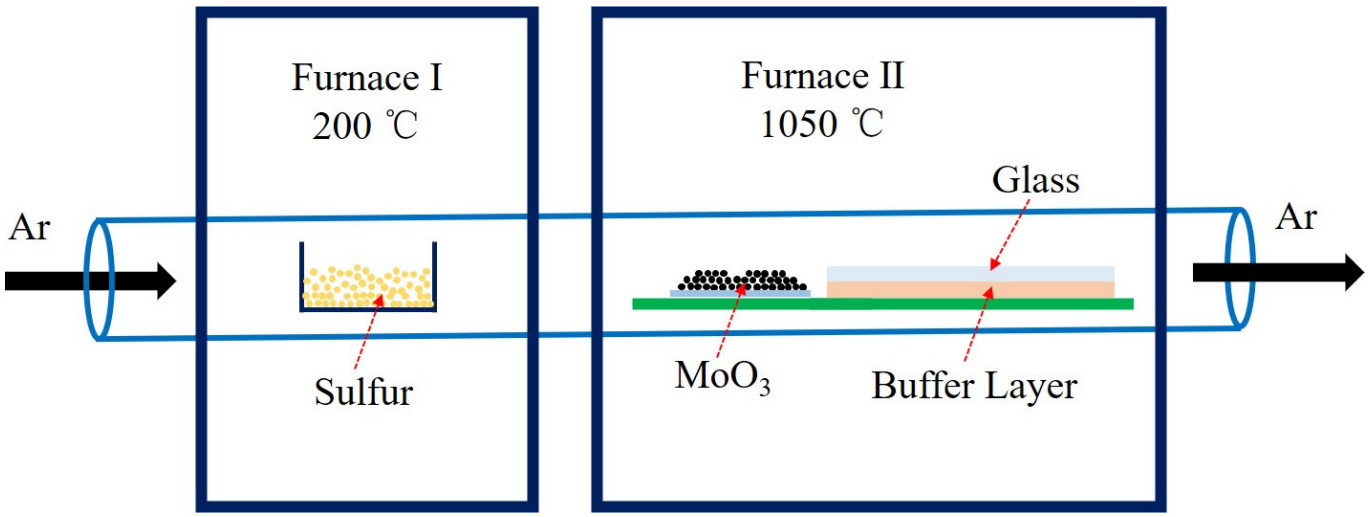

Figure 1. Schematic illustration of the CVD growth system setup.

3. Results and Discussion

Figure 2a,b are the optical photographs of glass/Mo and glass/Al_2O_3 substrates after the growth of MoS_2, respectively. The Mo foil buffer layer displays a color of gray, and the Al_2O_3 buffer layer shows different a color of white. Furthermore, the glass substrates shrunk obviously, and the edge of Mo foil and Al_2O_3 lamina showed up after the high-temperature growth process [23,26]. As we all know, the shape, distribution, and thickness of MoS_2 domains depend on the weight of precursors provided to the substrates. Consequently, as illustrated in Figure 2a,b, non-uniform MoS_2 film growth could be observed in different regions due to the different precursors' concentration distributions on the glass substrates [12,33,34]. Typically, in our growth setup, thicker continuous MoS_2 films could be grown upstream, closer to the Mo-source. Individual monolayer MoS_2 domains tend to be synthesized downstream, farther away from the Mo-source, and abundant growth phenomena could be observed in these regions. Therefore, in order to clearly demonstrate the advantages of glass/Al_2O_3 substrates, the MoS_2 morphology on the center and edge regions, as shown in Figure 2, was analyzed.

The MoS_2 domains grown on different regions of glass/Al_2O_3 and glass/Mo substrates are illustrated in Figures 3 and 4. Figure 3a,b are the typical optical microscopy images obtained from the MoS_2 domains grown on the center region of glass/Mo substrates. The MoS_2 domains exhibited triangle shapes and demonstrated lateral sizes larger than 400 μm, which is comparable to the MoS_2 domain sizes on glass substrates reported in other works [12,26]. The large crystal size could be attributed to the smooth, molten surface together with the catalytic role of the glass substrates, as reported in previous works [12,26,27,35,36]. As shown in Figure 3b, numerous tiny islands could be observed on the large MoS_2 triangle domains after additional magnification. The small bilayer islands could be attributed to the Mo foil buffer layer, which provides additional Mo-source during the growth of MoS_2 domains. Figure 3c,d are the representative optical microscopy images obtained from the MoS_2 domains grown on the center region of glass/Al_2O_3 substrates. Triangle MoS_2 domains larger than 400 μm with uniform color contrast could be observed.

In addition, no small bilayer islands could be observed on the amplified image of the MoS_2 domain, which demonstrates the thickness uniformity of MoS_2 crystal domains grown on the glass/Al_2O_3 substrates.

Figure 4 shows the MoS_2 domains on the edge of the glass/Mo and the glass/Al_2O_3 substrates. As shown in Figure 4a, the MoS_2 domains on the edge region of glass/Mo substrates generally exhibit star shapes with bright core centers. In contrast, the MoS_2 domains on the edge region of glass/Al_2O_3 substrates are sparse and generally exhibit triangle shapes with uniform thickness, as shown in Figure 4c. In addition, both the MoS_2 domains grown on glass/Mo and glass/Al_2O_3 were successfully transferred to SiO_2/Si substrates. Figure 4b shows the transferred MoS_2 domains with bright core centers that were grown on glass/Mo substrates. Figure 4d shows the transferred MoS_2 domains with uniform thickness that were grown on glass/Al_2O_3 substrates. The details of the transfer method have been reported in our previous works [24,25,37,38].

To provide a clear explanation of the different morphologies of the MoS_2 domains grown on glass/Mo and glass/Al_2O_3 substrates, a schematic illustration of the underlying growth mechanism was plotted. Typically, as shown in Figure 5a,b, the flat glass plane will be condensed into an oblate, sphere-like shape at a temperature higher than its molten point [23]. Subsequently, the Mo foil or Al_2O_3 buffer layer under glass substrates would be exposed to the CVD system. The Mo foil could be used as the Mo-source in the high-temperature CVD process, which has been demonstrated in previous work [26]. Therefore, excess Mo-source would be supplied and diffused on the glass/Mo substrates' surface. Consequently, the MoS_2 domains with small bilayer islands and bright core centers were grown at the center and edge regions, respectively. On the contrary, the strong chemical bonds of Al_2O_3 make it stable at high temperatures. Therefore, as shown in Figure 5c,d, the Al_2O_3 buffer layer would not affect the Mo-source supply during the process of MoS_2 growth and MoS_2 crystals with uniform thickness were grown. Furthermore, as discussed in previous works [12,26,27,35,36], the large domain size of MoS_2 at the center region of glass substrates could be ascribed to the smooth, molten glass surface under high temperature, together with the catalytic role of Na in the glass substrates, which reduce the energy barrier in the CVD process.

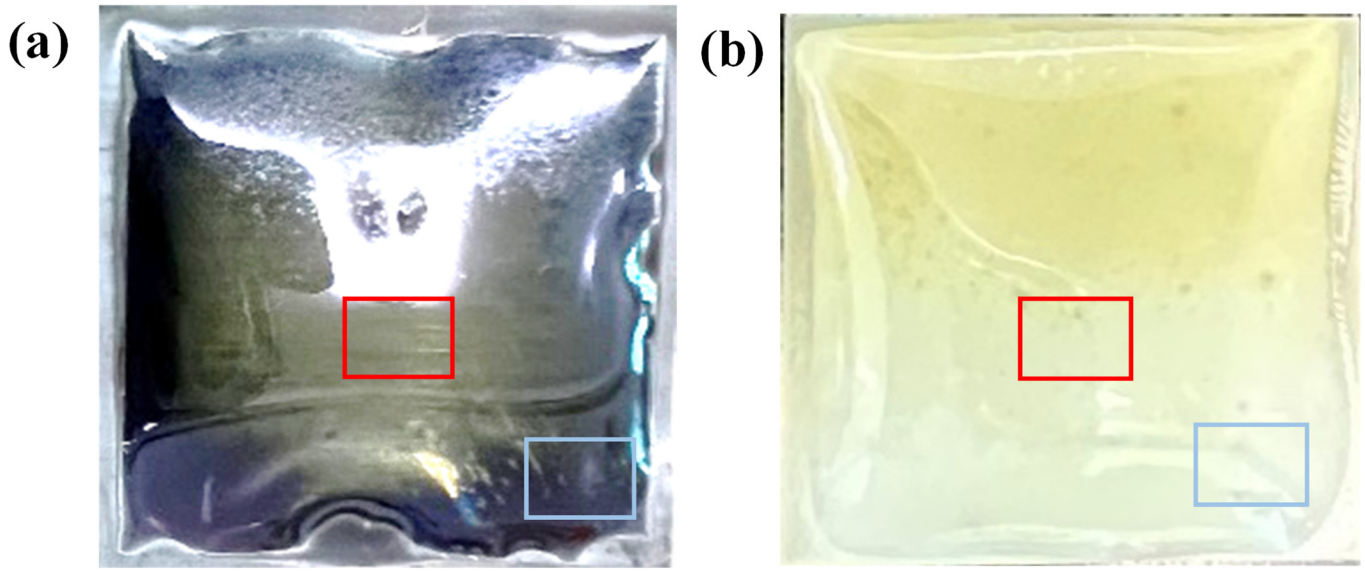

Figure 2. (**a**) Optical photograph of the glass/Mo substrates after the growth of MoS_2. (**b**) Optical photograph of the glass/Al_2O_3 substrates after the growth of MoS_2. The red rectangle corresponds to the center region, and the blue rectangle corresponds to the edge region.

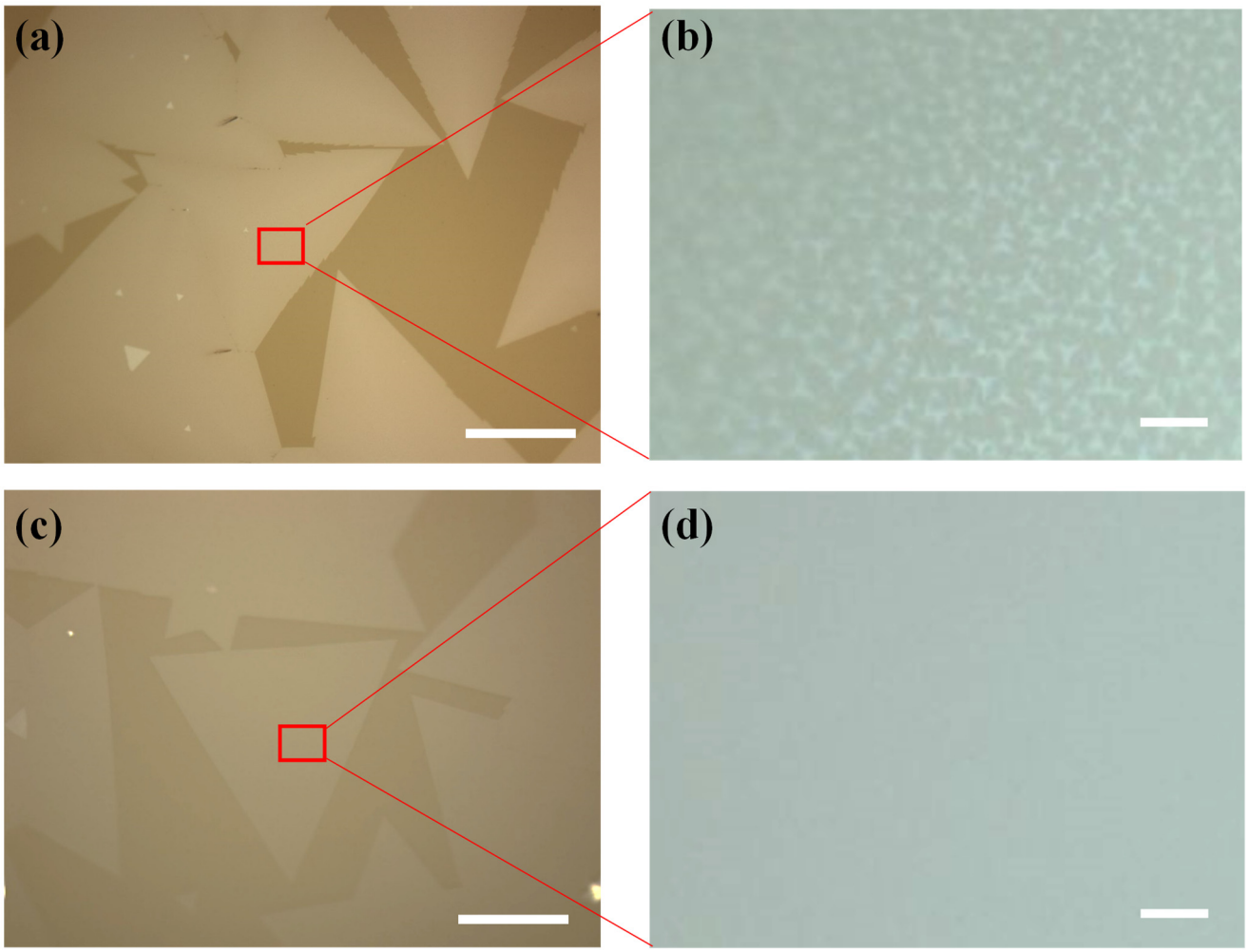

Figure 3. (**a**,**b**) Optical microscope images of the MoS_2 domains synthesized on the center region of glass/Mo substrates. (**c**,**d**) Optical microscope images of the MoS_2 domains synthesized on the center region of glass/Al_2O_3 substrates. Scale bar represents 200 μm for (**a**,**c**), and 10 μm for (**b**,**d**).

Raman spectroscopy is one commonly used spectroscopic technique to investigate phonons as well as the vibrational, rotational and other low-frequency modes in two-dimensional materials, which could be used to provide information about both crystal quality as well as estimate the number of layers of MoS_2 domains [39–42]. Therefore, Raman spectra were collected to further characterize the properties of MoS_2 grown on glass/Mo and glass/Al_2O_3. Figure 6a,c display the Raman spectra of the transferred MoS_2 domains on SiO_2/Si substrates that were grown on the center regions of glass/Mo and glass/Al_2O_3 substrates, respectively. As shown in Figure 6a, two characteristic Raman peaks were found at 385.4 cm^{-1} and 405.2 cm^{-1} in the spectral range, which can be assigned to in-plane vibration modes of Mo and S in the opposite direction ($E^1{}_{2g}$) and an out-of-plane vibration mode of S atoms (A_{1g}). The frequency difference for the MoS_2 domains grown on glass/Mo substrates was 19.7 cm^{-1}. For the MoS_2 domains grown on glass/Al_2O_3 substrates, the $E^1{}_{2g}$ and A_{1g} peaks are located at 387.3 cm^{-1} and 405.2 cm^{-1}. Compared with the MoS_2 domains grown on glass/Mo substrates, the frequency difference was reduced to 17.9 cm^{-1}, indicating a monolayer thickness for the measured MoS_2 domains. Moreover, the full width at half maximum (FWHM) of the $E^1{}_{2g}$ peak also reduced from 5.6 cm^{-1} to 3.8 cm^{-1}, demonstrating the high quality of the MoS_2 domains grown on glass/Al_2O_3 substrates. The reduced frequency difference and FWHM results from the different morphologies of MoS_2 domains grown on glass/Mo and glass/Al_2O_3 substrates,

as shown in Figure 3. In addition, PL spectroscopy was performed for the transferred MoS_2 domains grown on glass/Mo and glass/Al_2O_3 substrates, and the obtained spectra are shown in Figure 6b,d. Both those two types of MoS_2 have a characteristic peak (A exciton peak) at 1.84 eV, which is in agreement with previous studies [24,25]. The FWHMs of the A exciton peaks for MoS_2 domains grown on glass/Mo and glass/Al_2O_3 substrates are 1.02 and 0.96 eV, respectively. The reduced PL FWHMs of MoS_2 domains grown on glass/Al_2O_3 could also be attributed to its uniform thickness and high crystal quality.

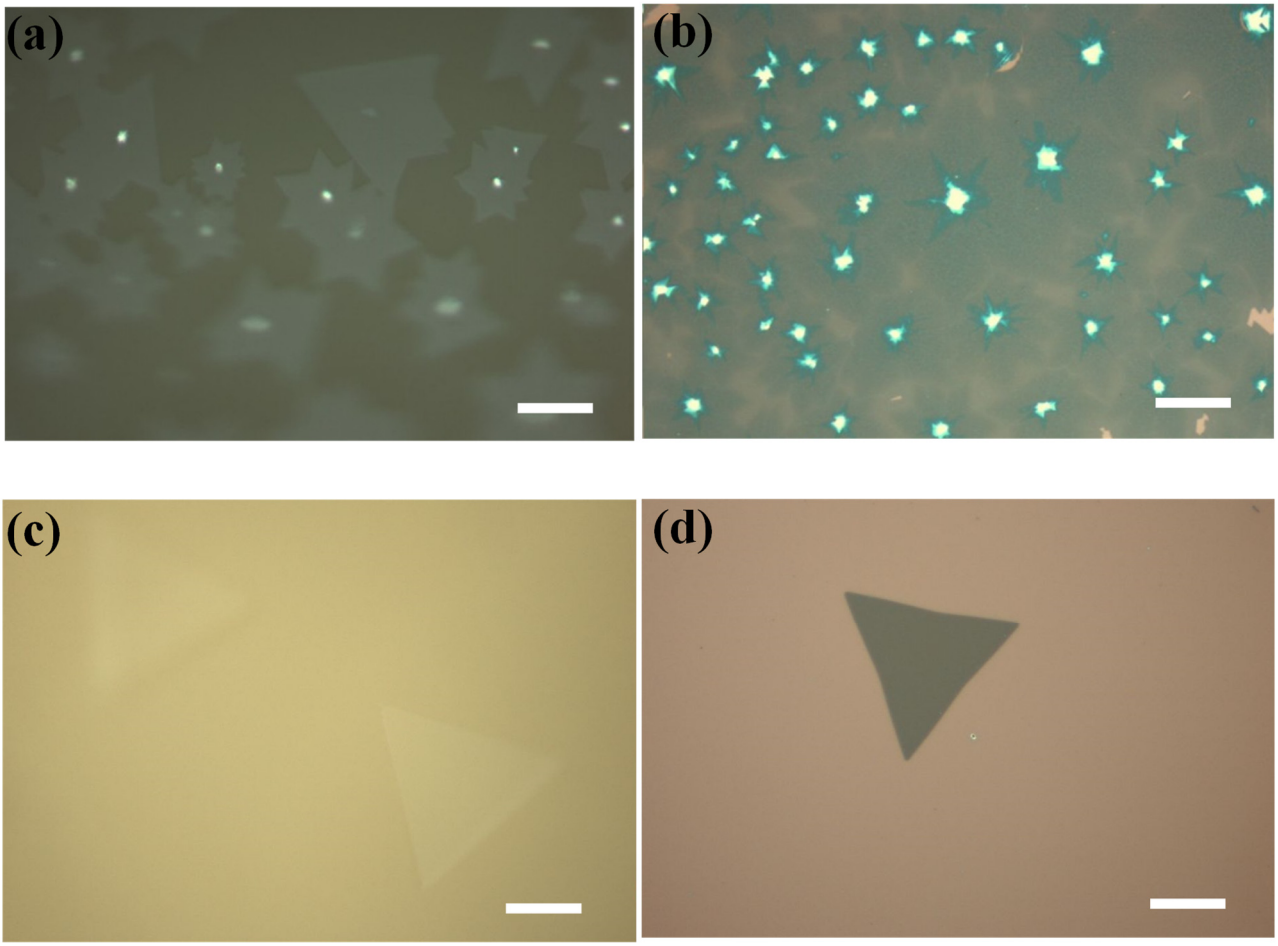

Figure 4. (**a**,**b**) Optical microscope images of the MoS_2 domains synthesized on the edge region of glass/Mo substrates. (**c**,**d**) Optical microscope images of the MoS_2 domains synthesized on the edge region of glass/Al_2O_3 substrates. Scale bar represents 50 μm for (**a**–**d**).

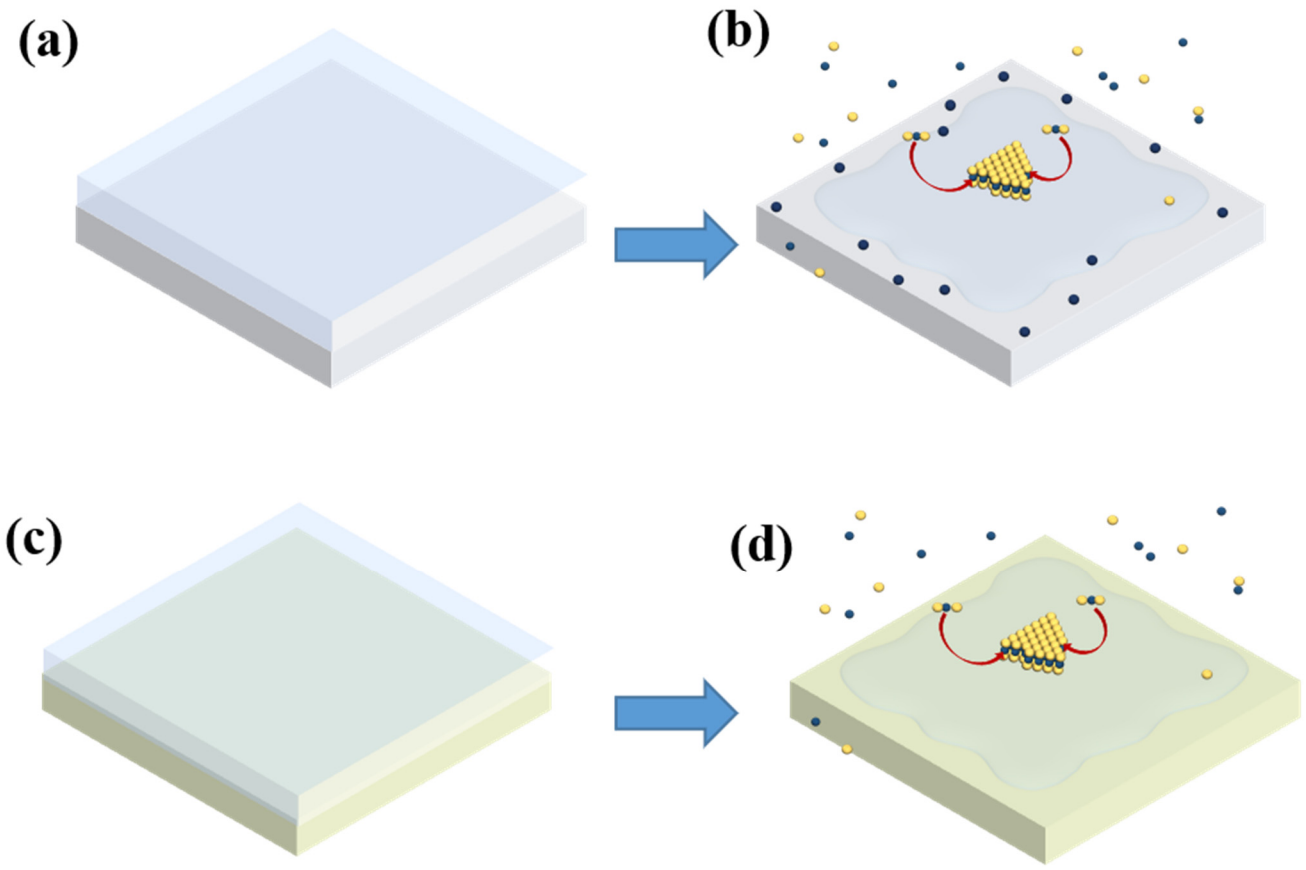

Figure 5. (**a**,**b**) Schematic illustration of the CVD growth process on glass/Mo substrates. (**c**,**d**) Schematic illustration of the CVD growth process on glass/Al_2O_3 substrates. The blue balls and yellow balls in (**b**,**d**) represent Mo and S atoms, respectively.

In order to further characterize the MoS_2 domains grown on glass/Al_2O_3 substrates, atomic force microscopy (AFM) and Raman mapping were performed after they were transferred onto SiO_2/Si substrates. Figure 7a displays the AFM images obtained from a typical triangle-shaped MoS_2 domain. A thickness of 0.7 nm was demonstrated through the AFM characterization, as shown in Figure 7b. This is consistent with the thickness of the monolayer MoS_2. Figure S1 displays the optical microscope and AFM images of the CVD-grown MoS_2 on the center region of glass/Al_2O_3 substrates. As shown in Figure S1b, numerous tiny islands could be observed on the large MoS_2 triangle domains. Figure 7c,d show the Raman intensity mappings recorded at 387.3 cm^{-1} and 405.2 cm^{-1}, respectively. The Raman mappings on the intensity of $E^1{}_{2g}$ mode and A_{1g} mode reveal a uniform color contrast, further demonstrating the thickness uniformity and good crystallinity of MoS_2 grown on glass/Al_2O_3 substrates.

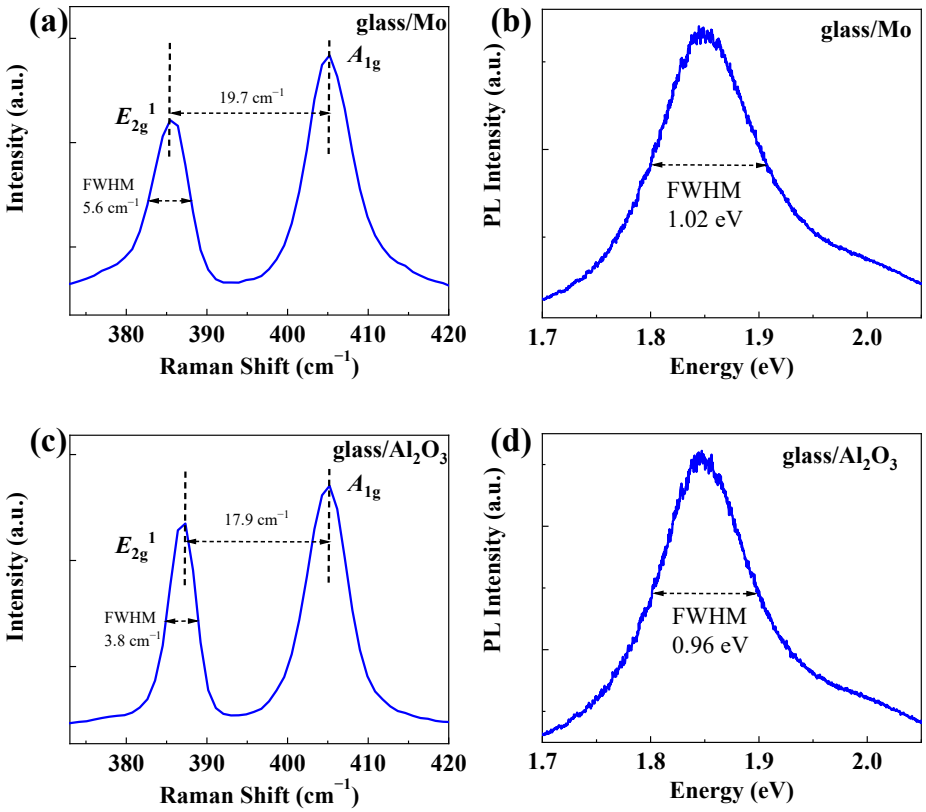

Figure 6. (**a**,**b**) Raman and PL spectral of the CVD-grown MoS_2 on the center region of glass/Mo substrates. (**c**,**d**) Raman and PL spectral of the CVD-grown MoS_2 on the center region of glass/Al_2O_3 substrates.

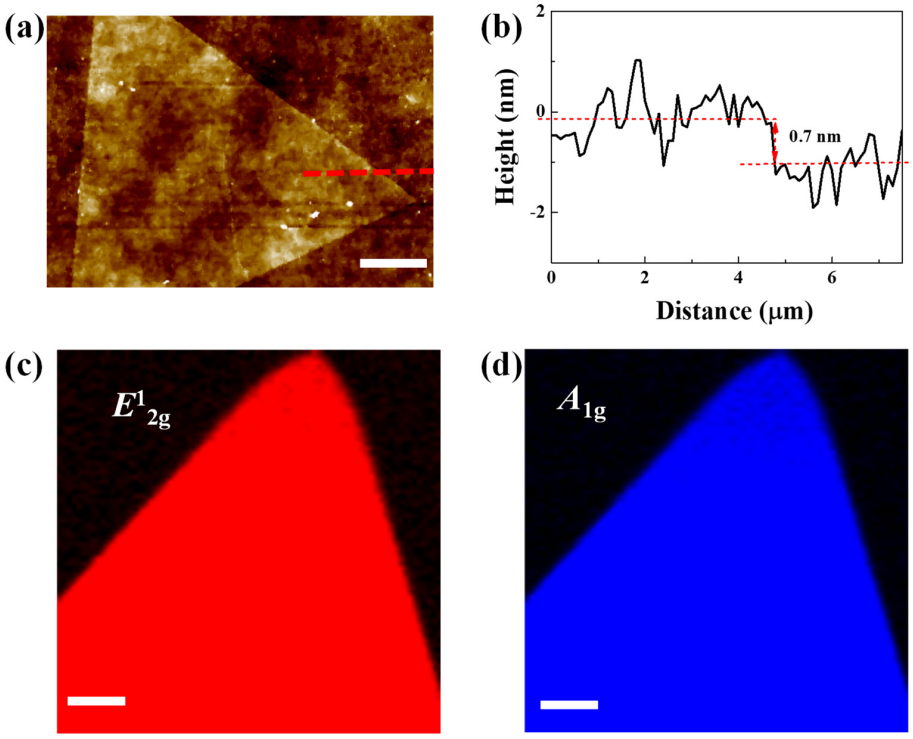

Figure 7. (**a**,**b**) AFM image and height profile of the CVD-grown MoS_2 on glass/Al_2O_3 substrates. (**c**,**d**) Raman mapping of the CVD-grown MoS_2 on glass/Al_2O_3 substrates. Scale bar are 5 μm for (**a**), and Scale bars are 3 μm for (**c**,**d**).

4. Conclusions

In this work, the two-dimensional semiconductor MoS_2 was successfully synthesized on glass/Al_2O_3 substrates for the first time. The advantages of glass/Al_2O_3 substrates for CVD MoS_2 growth were demonstrated by a direct comparison of glass/Mo substrates. Optical microscopy revealed that MoS_2 crystals grown on both glass/Mo and glass/Al_2O_3 substrates were conventionally triangle-shaped and had a lateral size larger than 400 μm. Numerous bilayer islands and bright core centers could be observed on the surface of MoS_2 domains at the center region and edge region of glass/Mo substrates. As a control, MoS_2 domains grown on glass/Al_2O_3 substrates exhibited uniform optical contrast, demonstrating the thickness uniformity of those MoS_2 domains. The Raman and PL comparison of MoS_2 domains further confirmed this. In addition, the thickness of MoS_2 domains was characterized by atomic force microscopy and the homogeneity of MoS_2 domains grown on glass/Al_2O_3 substrates was further demonstrated by Raman mapping. These results demonstrate a novel method to produce MoS_2 films on glass substrates and are of great value for future commercial applications of MoS_2 films.

Supplementary Materials: The following supporting information can be downloaded at: https://www.mdpi.com/article/10.3390/nano12152719/s1, Figure S1: AFM image of the CVD growth MoS_2 on glass/Mo substrates.

Author Contributions: Conceptualization, Q.G.; methodology, Q.G., J.L., L.C., Z.X. and S.C.; validation, Q.G. and S.C.; formal analysis, Q.G.; investigation, Q.G., S.C. and L.C.; resources, Q.G., P.L., X.Z. and W.C.; data curation, Q.G.; writing—original draft preparation, Q.G.; writing—review and editing, Q.G.; visualization, Q.G., D.L. and S.X.; supervision, Q.G.; project administration, Q.G. and C.Z.; funding acquisition, Q.G. and C.Z. All authors have read and agreed to the published version of the manuscript.

Funding: This work was funded in part by the Natural Science Foundation of China (Grant Nos. 62104033, 62071088 and 11775047), in part by the Guangdong Basic and Applied Basic Research Foundation (Grant No. 2019A1515110752), in part by the Youth Innovative Talent Project of Guangdong Education Department (Grant No. 2019KQNCX187), in part by the Outstanding Chinese and Foreign Youth Exchange Program of China Association for Science and Technology (CAST) 2019, in part by the Project for Innovation Team of Guangdong University (Grant Nos. 2018KCXTD033, 2020KCXTD030 and 2021KCXTD040), in part by the Construction Project of Professional Quality Engineering in 2022 (Grant No. YLZY202201), in part by the key scientific research project of the Department of Education of Guangdong Province (Grant No. 2021ZDZX1052), and in part by National Key R&D Program of China (Grant No. 2018YFB1801302).

Data Availability Statement: The data that support the findings of this study are available from the corresponding author upon reasonable request.

Conflicts of Interest: The authors declare no conflict of interest.

References

1. Wu, F.; Tian, H.; Shen, Y.; Hou, Z.; Ren, J.; Gou, G.; Sun, Y.; Yang, Y.; Ren, T.-L. Vertical MoS2 transistors with sub-1-nm gate lengths. *Nature* **2022**, *603*, 259–264. [CrossRef] [PubMed]
2. Shen, P.-C.; Su, C.; Lin, Y.; Chou, A.-S.; Cheng, C.-C.; Park, J.-H.; Chiu, M.-H.; Lu, A.-Y.; Tang, H.-L.; Tavakoli, M.M.; et al. Ultralow contact resistance between semimetal and monolayer semiconductors. *Nature* **2021**, *593*, 211–217. [CrossRef]
3. Meng, W.; Xu, F.; Yu, Z.; Tao, T.; Shao, L.; Liu, L.; Li, T.; Wen, K.; Wang, J.; He, L.; et al. Three-dimensional monolithic micro-LED display driven by atomically thin transistor matrix. *Nat. Nanotechnol.* **2021**, *16*, 1231–1236. [CrossRef] [PubMed]
4. Zhang, X.; Grajal, J.; Vazquez-Roy, J.L.; Radhakrishna, U.; Wang, X.; Chern, W.; Zhou, L.; Lin, Y.; Shen, P.-C.; Ji, X.; et al. Two-dimensional MoS2-enabled flexible rectenna for Wi-Fi-band wireless energy harvesting. *Nature* **2019**, *566*, 368–372. [CrossRef] [PubMed]
5. Lin, Z.; Liu, Y.; Halim, U.; Ding, M.; Liu, Y.; Wang, Y.; Jia, C.; Chen, P.; Duan, X.; Wang, C.; et al. Solution-processable 2D semiconductors for high-performance large-area electronics. *Nature* **2018**, *562*, 254–258. [CrossRef] [PubMed]
6. Desai, S.B.; Madhvapathy, S.R.; Sachid, A.B.; Llinas, J.P.; Wang, Q.; Ahn, G.H.; Pitner, G.; Kim, M.J.; Bokor, J.; Hu, C.; et al. MoS_2 transistors with 1-nanometer gate lengths. *Science* **2016**, *354*, 99–102. [CrossRef]
7. Akinwande, D.; Petrone, N.; Hone, J. Two-dimensional flexible nanoelectronics. *Nat. Commun.* **2014**, *5*, 5678. [CrossRef]

8. Li, T.; Guo, W.; Ma, L.; Li, W.; Yu, Z.; Han, Z.; Gao, S.; Liu, L.; Fan, D.; Wang, Z.; et al. Epitaxial growth of wafer-scale molybdenum disulfide semiconductor single crystals on sapphire. *Nat. Nanotechnol.* **2021**, *16*, 1201–1207. [CrossRef]
9. Liu, L.; Li, T.; Ma, L.; Li, W.; Gao, S.; Sun, W.; Dong, R.; Zou, X.; Fan, D.; Shao, L.; et al. Uniform nucleation and epitaxy of bilayer molybdenum disulfide on sapphire. *Nature* **2022**, *605*, 69–75. [CrossRef]
10. Yang, P.; Zhang, S.; Pan, S.; Tang, B.; Liang, Y.; Zhao, X.; Zhang, Z.; Shi, J.; Huan, Y.; Shi, Y.; et al. Epitaxial Growth of Centimeter-Scale Single-Crystal MoS_2 Monolayer on Au(111). *ACS Nano* **2020**, *14*, 5036–5045. [CrossRef]
11. Wang, Q.; Li, N.; Tang, J.; Zhu, J.; Zhang, Q.; Jia, Q.; Lu, Y.; Wei, Z.; Yu, H.; Zhao, Y.; et al. Wafer-Scale Highly Oriented Monolayer MoS_2 with Large Domain Sizes. *Nano Lett.* **2020**, *20*, 7193–7199. [CrossRef] [PubMed]
12. Yang, P.; Zou, X.; Zhang, Z.; Zhongfan, L.; Shi, J.; Chen, S.; Shulin, C.; Zhao, L.; Jiang, S.; Zhou, X.; et al. Batch production of 6-inch uniform monolayer molybdenum disulfide catalyzed by sodium in glass. *Nat. Commun.* **2018**, *9*, 979. [CrossRef] [PubMed]
13. Yu, H.; Liao, M.; Zhao, W.; Liu, G.; Zhou, X.J.; Wei, Z.; Xu, X.; Liu, K.; Hu, Z.; Deng, K.; et al. Wafer-Scale Growth and Transfer of Highly-Oriented Monolayer MoS_2 Continuous Films. *ACS Nano* **2017**, *11*, 12001–12007. [CrossRef]
14. Zhou, J.; Lin, J.; Huang, X.; Zhou, Y.; Chen, Y.; Xia, J.; Wang, H.; Xie, Y.; Yu, H.; Lei, J.; et al. A library of atomically thin metal chalcogenides. *Nature* **2018**, *556*, 355–359. [CrossRef] [PubMed]
15. Ji, Q.; Su, C.; Mao, N.; Tian, X.; Idrobo, J.-C.; Miao, J.; Tisdale, W.A.; Zettl, A.; Li, J.; Kong, J. Revealing the Brønsted-Evans-Polanyi relation in halide-activated fast MoS_2 growth toward millimeter-sized 2D crystals. *Sci. Adv.* **2021**, *7*, eabj3274. [CrossRef] [PubMed]
16. Zhang, L.; Dong, J.; Ding, F. Strategies, Status, and Challenges in Wafer Scale Single Crystalline Two-Dimensional Materials Synthesis. *Chem. Rev.* **2021**, *121*, 6321–6372. [CrossRef] [PubMed]
17. Li, S. Salt-assisted chemical vapor deposition of two-dimensional transition metal dichalcogenides. *iScience* **2021**, *24*, 103229. [CrossRef]
18. Zhou, S.; Jiao, L. Growth of Single-crystalline Transition Metal Dichalcogenides Monolayers with Large-size. *Chem. Res. Chin. Univ.* **2020**, *36*, 511–517. [CrossRef]
19. Xu, X.; Zhang, Z.; Qiu, L.; Zhuang, J.; Zhang, L.; Wang, H.; Liao, C.; Song, H.; Qiao, R.; Gao, P.; et al. Ultrafast growth of single-crystal graphene assisted by a continuous oxygen supply. *Nat. Nanotechnol.* **2016**, *11*, 930–935. [CrossRef]
20. Zhang, Z.; Xu, X.; Qiu, L.; Wang, S.; Wu, T.; Ding, F.; Peng, H.; Liu, K. The Way towards Ultrafast Growth of Single-Crystal Graphene on Copper. *Adv. Sci.* **2017**, *4*, 1700087. [CrossRef]
21. Xiong, L.; Wang, K.; Li, D.; Luo, X.; Weng, J.; Liu, Z.; Zhang, H. Research progress on the preparations, characterizations and applications of large scale 2D transition metal dichalcogenides films. *FlatChem* **2020**, *21*, 100161. [CrossRef]
22. Li, Q.; Zhang, L.; Li, C.; He, J.; Wei, Y.; Zhao, J.; Zhang, R.; Wang, P.; Fu, S.; Chen, F.; et al. Morphological Evolution of Monolayer MoS2 Single-Crystalline Flakes. *J. Phys. Chem. C* **2022**, *126*, 3549–3559. [CrossRef]
23. Zeng, M.; Liu, J.; Zhou, L.; Mendes, R.G.; Dong, Y.; Zhang, M.-Y.; Cui, Z.-H.; Cai, Z.; Zhang, Z.; Zhu, D.; et al. Bandgap tuning of two-dimensional materials by sphere diameter engineering. *Nat. Mater.* **2020**, *19*, 528–533. [CrossRef] [PubMed]
24. Zhang, Z.; Xu, X.; Song, J.; Gao, Q.; Li, S.; Hu, Q.; Li, X.; Wu, Y. High-performance transistors based on monolayer CVD MoS_2 grown on molten glass. *Appl. Phys. Lett.* **2018**, *113*, 202103. [CrossRef]
25. Gao, Q.; Zhang, Z.; Xu, X.; Song, J.; Li, X.; Wu, Y. Scalable high performance radio frequency electronics based on large domain bilayer MoS2. *Nat. Commun.* **2018**, *9*, 4778. [CrossRef]
26. Chen, J.; Zhao, X.; Grinblat, G.; Chen, Z.; Tan, S.J.R.; Fu, W.; Ding, Z.; Abdelwahab, I.; Li, Y.; Geng, D.; et al. Homoepitaxial Growth of Large-Scale Highly Organized Transition Metal Dichalcogenide Patterns. *Adv. Mater.* **2017**, *30*, 1704674. [CrossRef] [PubMed]
27. Chen, J.; Zhao, X.; Tan, S.J.R.; Xu, H.; Wu, B.; Liu, B.; Fu, D.; Fu, W.; Geng, D.; Liu, Y.; et al. Chemical Vapor Deposition of Large-Size Monolayer $MoSe_2$ Crystals on Molten Glass. *J. Am. Chem. Soc.* **2017**, *139*, 1073–1076. [CrossRef]
28. Cai, Z.; Lai, Y.; Zhao, S.; Zhang, R.; Tan, J.; Feng, S.; Zou, J.; Tang, L.; Lin, J.; Liu, B.; et al. Dissolution-precipitation growth of uniform and clean two dimensional transition metal dichalcogenides. *Natl. Sci. Rev.* **2020**, *8*, 115. [CrossRef]
29. Tang, J.; Wei, Z.; Wang, Q.; Wang, Y.; Han, B.; Li, X.; Huang, B.; Liao, M.; Liu, J.; Li, N.; et al. In Situ Oxygen Doping of Monolayer MoS_2 for Novel Electronics. *Small* **2020**, *16*, 2004276. [CrossRef]
30. Durairaj, S.; Ponnusamy, K.; Shinde, N.B.; Eswaran, S.K.; Asokan, V.; Park, J.B.; Chandramohan, S. Oxygen-Driven Growth Regulation and Defect Passivation in Chemical Vapor Deposited MoS_2 Monolayers. *Cryst. Growth Des.* **2021**, *21*, 6793–6801. [CrossRef]
31. Yao, B.; Li, R.; Zhang, C.; Zhou, Z.; Fu, Z.; Huang, X.; Yuan, G.; Xu, J.; Gao, L. Tuning the morphology of 2D transition metal chalcogenides via oxidizing conditions. *J. Physics Condens. Matter* **2022**, *34*, 195001. [CrossRef] [PubMed]
32. Chen, W.; Zhao, J.; Zhang, J.; Gu, L.; Yang, Z.; Li, X.; Yu, H.; Zhu, X.; Yang, R.; Shi, D.; et al. Oxygen-Assisted Chemical Vapor Deposition Growth of Large Single-Crystal and High-Quality Monolayer MoS_2. *J. Am. Chem. Soc.* **2015**, *137*, 15632–15635. [CrossRef] [PubMed]
33. Tang, L.; Li, T.; Luo, Y.; Feng, S.; Cai, Z.; Zhang, H.; Liu, B.; Cheng, H.-M. Vertical Chemical Vapor Deposition Growth of Highly Uniform 2D Transition Metal Dichalcogenides. *ACS Nano* **2020**, *14*, 4646–4653. [CrossRef]
34. Tang, L.; Tan, J.; Nong, H.; Liu, B.; Cheng, H.-M. Chemical Vapor Deposition Growth of Two-Dimensional Compound Materials: Controllability, Material Quality, and Growth Mechanism. *Accounts Mater. Res.* **2021**, *2*, 36–47. [CrossRef]

35. Zhang, Z.; Zhu, L.; Wang, D.; Tang, B.; Yang, P.; Shi, Y.; Zhou, F.; Fu, J.; Huan, Y.; Cui, F.; et al. Ultrafast Growth of Large-Area Uniform, Millimeter-Size MoSe $_2$ Single Crystals on Low-Cost Soda-Lime Glass. *Adv. Mater. Interfaces* **2021**, *8*, 2100415. [CrossRef]
36. Han, W.; Liu, K.; Yang, S.; Wang, F.; Su, J.; Jin, B.; Li, H.; Zhai, T. Salt-assisted chemical vapor deposition of two-dimensional materials. *Sci. China Ser. B Chem.* **2019**, *62*, 1300–1311. [CrossRef]
37. Gao, Q.; Zhang, C.; Yang, K.; Pan, X.; Zhang, Z.; Yang, J.; Yi, Z.; Chi, F.; Liu, L. High-Performance CVD Bilayer MoS_2 Radio Frequency Transistors and Gigahertz Mixers for Flexible Nanoelectronics. *Micromachines* **2021**, *12*, 451. [CrossRef]
38. Gao, Q.; Zhang, C.; Liu, P.; Hu, Y.; Yang, K.; Yi, Z.; Liu, L.; Pan, X.; Zhang, Z.; Yang, J.; et al. Effect of Back-Gate Voltage on the High-Frequency Performance of Dual-Gate MoS_2 Transistors. *Nanomaterials* **2021**, *11*, 1594. [CrossRef]
39. Wang, Y.; Cong, C.; Qiu, C.; Yu, T. Raman Spectroscopy Study of Lattice Vibration and Crystallographic Orientation of Monolayer MoS_2under Uniaxial Strain. *Small* **2013**, *9*, 2857–2861. [CrossRef]
40. Li, H.; Zhang, Q.; Yap, C.C.R.; Tay, B.K.; Edwin, T.H.T.; Olivier, A.; Baillargeat, D. From Bulk to Monolayer MoS2: Evolution of Raman Scattering. *Adv. Funct. Mater.* **2012**, *22*, 1385–1390. [CrossRef]
41. Chakraborty, B.; Bera, A.; Muthu, D.V.S.; Bhowmick, S.; Waghmare, U.V.; Sood, A.K. Symmetry-dependent phonon renormalization in monolayer MoS22transistor. *Phys. Rev. B* **2012**, *85*, 161403. [CrossRef]
42. Zobel, A.; Boson, A.; Wilson, P.M.; Muratov, D.S.; Kuznetsov, D.V.; Sinitskii, A. Chemical vapour deposition and characterization of uniform bilayer and trilayer MoS_2crystals. *J. Mater. Chem. C* **2016**, *4*, 11081–11087. [CrossRef]